Chemical Engineering Journal 164 (2010) 196–207

Contents lists available at ScienceDirect

Chemical Engineering Journal

journal homepage: www.elsevier.com/locate/cej

Sono-Fenton oxidation of formic acid/formate ions in an aqueous solution: From an experimental design to the mechanistic modeling

Ivana Grčić*, Monika Obradović, Dinko Vujević, Natalija Koprivanac

Faculty of Chemical Engineering and Technology, University of Zagreb, Marulićev Trg 19, HR-10000 Zagreb, Croatia

ARTICLE INFO

Article history:
Received 12 March 2010
Received in revised form 22 August 2010
Accepted 23 August 2010

Keywords:
Sonochemical Fenton oxidation
Persulfate Fenton
Formic acid
Oxalic acid
Experimental design
Mathematical modeling

ABSTRACT

In order to establish an efficient oxidation process for the mineralization of a model wastewater containing formate species, the effects of some operating parameters such as Fenton reagent dosages and volume of the treated system were observed during the treatment by the ultrasonic assisted Fenton and modified Fenton processes. The mineralization kinetics was also examined based on the experimental data. The overall mineralization kinetics was found to be in the accordance with the first-order reaction kinetics.

The results obtained within this work indicate an efficient mineralization, achieved by studied sonochemical oxidation processes. With the appropriate combination of operating parameters it is reasonable to expect a mineralization extent of 94%, corresponding to the complete degradation of formate species with the consequent formation and the degradation of oxalic acid in the system.

The detailed mathematical model describing the ongoing process in the studies batch system was developed on the basis of a mechanistic reaction scheme, given in the frame of this work. The model has been validated, pointing at the significance of the assumed reactions and the accuracy of the corresponding rate constants.

1. Introduction

An active interest for studying the new technologies for a possible implementation in wastewater treatment, grew from the urge for elimination of hazardous pollutants from industrial effluents. Wastewaters originating from petrochemical industries are considered as very complex and hard to treat, with the constituents that are highly specific [1]. The versatility of advanced oxidation processes (AOPs) enhanced by the fact that they offer different possible ways for highly reactive radicals' production and a consecutive mineralization of wastewaters, allows a better compliance with the specific requirements of the environmental and other regulatives [2]. Sonochemical treatment has been found to be the one of the successful technologies for a degradation of various organic pollutants due to the emphasised cavitational activity [3]. However, total mineralization of organic pollutants by means of ultrasound irradiation alone still remains a difficult task and thus application of ultrasound for an industrial plant is still impractical. To overcome the limitation of low degradation efficiency, many efforts have been made on investigation of various combined ultrasonic systems in order to reach a desired efficiency of substrate and total carbon degradation and reduce the reaction time required for removing the pollutants [4]. These methods include ultrasound coupled technologies with oxidants such as hydrogen peroxide (H_2O_2) [5,6] and ozone [7], electrochemical methods [8], Fenton reagent [9–11] and photocatalysis [12,13], and other catalytic oxidation processes [14,15].

The scope of this study was to evaluate the application of ultrasonic (US) assisted AOPs and a development of a representative mathematical model. US assisted Fenton process and US assisted modified Fenton process, US/Fe^{2+}/H_2O_2 and US/Fe^{2+}/$S_2O_8^{2-}$ respectively, were applied for the treatment of model wastewaters containing formate ions that is considered as the major contaminant in industrial wastewater originating from 1,2-DCA/VCM plant [1]. Since previous study [11] as well as the preliminary results discussed in this work have confirmed that by application of US/Fe^{3+}/H_2O_2 and US/Fe^{3+}/$S_2O_8^{2-}$ process among all other studied processes, the highest mineralization extent in the investigated wastewater system was obtained, these two processes were the subject for further more detailed analyses. Furthermore, due to the high standard redox potential of sulfate radicals, $SO_4^{\bullet-}$ (E = 3.1 V), compared to the most common oxidant, hydroxyl radical, $^{\bullet}OH$ (E = 2.72 V), an active interest in the sulfate radical based AOPs is present [16–18].

To establish the effects of the operating parameters and to optimize the applied process in the terms of reagents

* Corresponding author. Tel.: +385 1 4597 123; fax: +385 1 4597 143.
E-mail address: igrcic@fkit.hr (I. Grčić).

1385-8947/$ – see front matter © 2010 Elsevier B.V. All rights reserved.
doi:10.1016/j.cej.2010.08.059

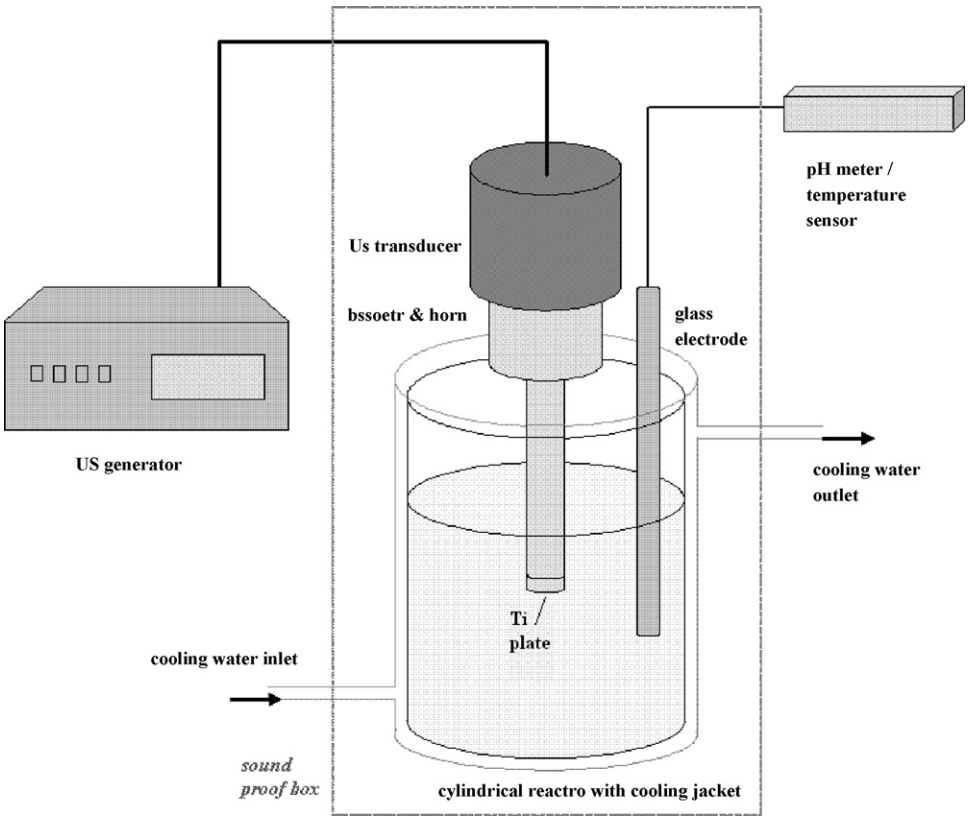

Fig. 1. Scheme of the reactor used for the experiments involving the sonication.

consumption and an involved energy, i.e. ultrasonic power, corresponding to the treated volume, the statistical study of formate degradation was performed applying Box–Behnken experimental design for US/Fe^{2+}/H_2O_2 process, and 3 level factorial design for US/Fe^{2+}/$S_2O_8{}^{2-}$ process. Predictive models were developed and the effect of each parameter determined. Furthermore, single-response optimization was attempted through desirability function based on the developed predictive models [1]. The kinetics of formate degradation in studied systems was investigated, which led to the development of mathematical models according to the mechanistic degradation scheme. The applied mechanistic scheme was based on the part of the previous study [1,11] and on a lot of relevant data [11,16,19–26]. All the reaction occurring in the studied systems were grouped as follows; reactions of the Fenton catalytic cycle (i), ultrasonic induced reactions (ii), free radical propagation and termination reactions (iii) and formic/formate oxidation scheme (iv). Within the proposed oxidation scheme, the main assumption was the formation of the oxalic acid due to propagation reaction over the carboxyl cage, Eqs. (1) and (2) [20,27,28].

$$HO^{\bullet -} + HCO_2^- \longrightarrow H_2O + CO_2^{\bullet -} \quad (1)$$

$$CO_2^{\bullet -} + CO_2^{\bullet -} \leftrightarrow [CO_2^{\bullet -} \cdots CO_2^{\bullet -}] \rightarrow \text{-O-C(=O)-C(=O)-O-} + CO_2 \quad (2)$$

The developed mechanistical model has been tested and successfully validated via independent set of the experiments. The competitiveness of the model reactions and the role of the ultrasound will be discussed later.

2. Materials and methods

2.1. Chemicals

All reagents used in this work were analytical or HPLC grade and used without any further purification. Ferrous sulfate ($FeSO_4{\cdot}(7H_2O)$), ferric sulfate ($Fe_2(SO_4)_3{\cdot}(H_2O)$), hydrogen peroxide ($H_2O_2$ 30%), potassium persulfate ($K_2S_2O_8$), potassium iodide (KI 1%), ferrous ammonium sulfate ($(NH_4)_2Fe(SO4)_2{\cdot}(6H_2O)$), ammonium thiocyanate (NH_4SCN), potassium hydroxide (KOH) and sulfuric acid (H_2SO_4 50%) were supplied by Kemika, Zagreb, Croatia. Sodium formate (HCOONa), ammonium metavanadate (NH_4VO_3), and ortho-phosphoric acid (H_3PO_4 85%) were obtained from Sigma–Aldrich.

2.2. Experimental apparatus

A schematic drawing of the reactor used for the experiments involving the sonication is shown in Fig. 1. An ultrasonic homogenizer SONOPLUS HD 2200 (Bandelin, Germany) consisted of a generator, ultrasonic converter (model SH70G; including transducer, booster and horn) and a probe tip (thin plate) made of titanium alloy (TT13; 13 mm in diameter) operated at 20 kHz. The amplitude in the performed experiments was adjusted at 100% (200 W power output) continuously, without pulse length setup. Experiments were performed in a cylindrical batch reactor made from borosilicate glass with the cooling jacket and the maximum working volume of 0.75 L. The ultrasonic probe was placed vertically in the middle of the reactor. The temperature of the system was monitored during the sonication time and kept constant, $29 \pm 3\,^{\circ}C$. Temperature and pH of the system were continuously monitored by pH/conductivity meter with the integrated NTC 30/Pt1000 temperature sensor (Handylab LF 12, Schott, Germany). The position of the sensor was fixed at a middle distance

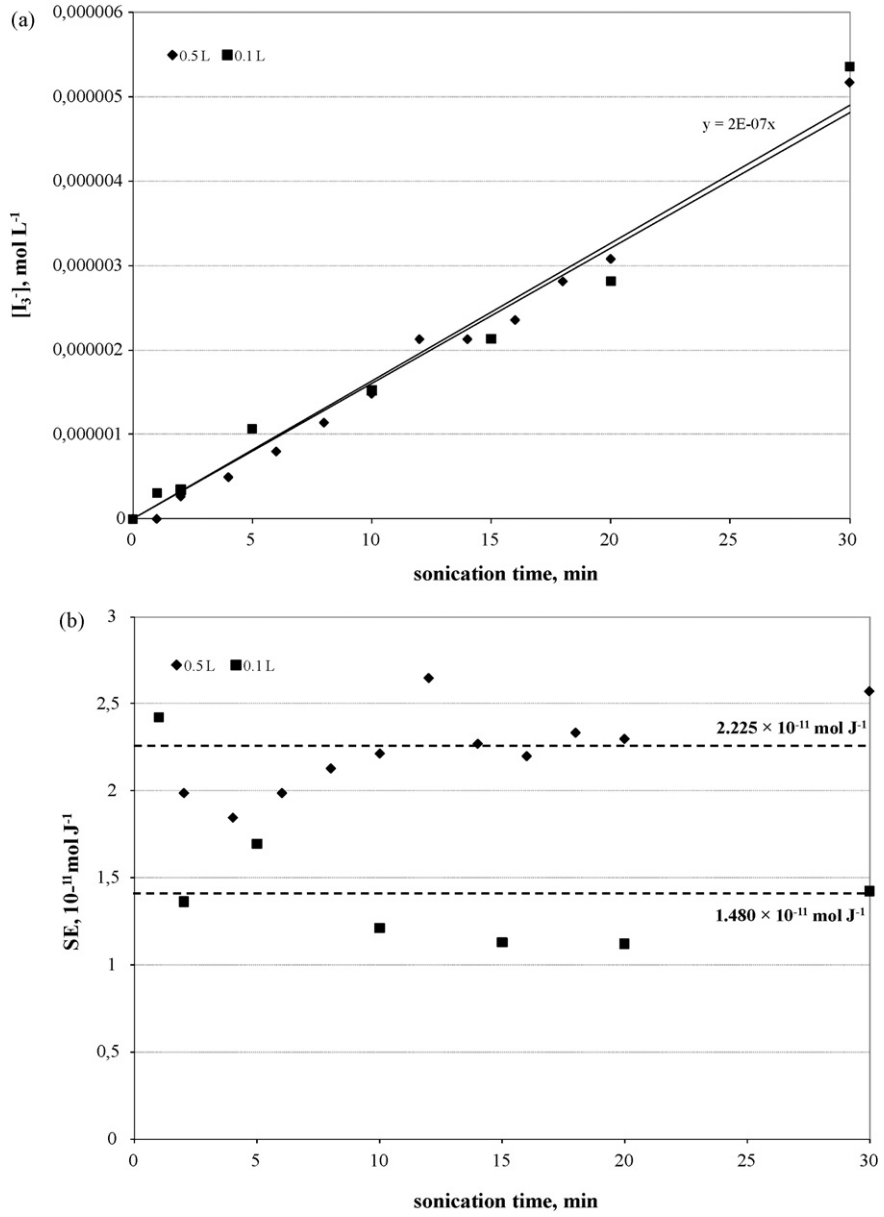

Fig. 2. Determination of the cavitational activity in the different reaction volumes; triiodide formation during the sonication of the KI solution (0.1 mol L^{-1}) (a) and sonochemical efficiency determined at the operating conditions; 20 kHz, 200 W electric input, 29 ± 3 °C.

between the probe and a rector wall, immersed in the solution approximately 1 cm below the probe level. No additional mixing was introduced to the system. Experiments that assumed performing of the processes in the smaller volume (0.1 and 0.3 L) were made in the ice-water bath cooled glass reaction vessels whose geometry (diameter to height ratio) was similar to the cylindrical batch reactor described previously.

Experiments without sonication were performed as jar-tests in glass reaction vessels with the maximum reaction volume of 0.6 L and constant magnetic stirring (650 rpm) in a thermostated bath, 29 ± 2 °C.

The experiment involving the employment of UV-C light was performed in a batch photo reactor of 0.8 L total volume. The reactor was made of borosilicate glass, with sampling ports on the top, magnetic stirrer and water jacket for temperature control [29]. The irradiation source was low pressure mercury UV lamp (PenRay 90-0012-01), UV-C 254 nm, UVP-Ultra Violet Products, Cambridge, UK) with typical intensity of 4.4 W cm^{-2} (λ = 254 nm) at 2 cm distance of the source. UV lamp was placed axially in a quartz tube inside the reactor. The reaction temperature was also kept at 29 ± 2 °C.

2.3. Experimental procedure

The model solution was prepared by dissolving sodium formate in distilled water (in concentration of 250 mg L^{-1}, otherwise indicated). The initial pH of the studied system was adjusted at 3 (optimal pH value for Fenton oxidations [1,30], using sulfuric acid (1 mol L^{-1}), which was followed by the addition of iron salt and hydrogen peroxide or potassium persulfate. Experiments were carried on for 30 min. Samples were taken out every 5 min (otherwise indicated); in a typical experiment, a grain or two of KOH was added in each sample in order to precipitate hydroxides of iron and to ensure the non-reaction after sampling. Samples were then subjected to further analyses. When investigating the corresponding ferrous/ferric ions concentration in the system with the time, a

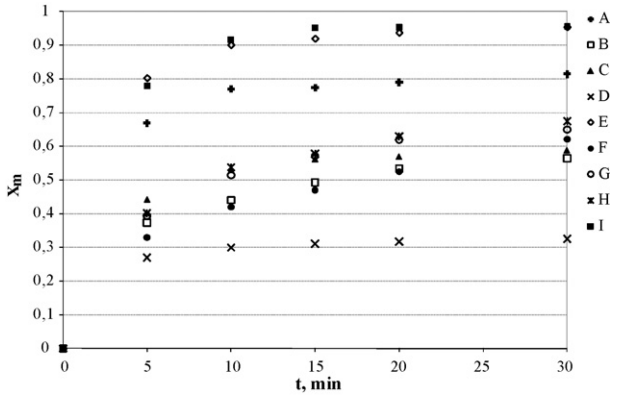

Fig. 3. Conversions achieved by different processes (A – Fe^{2+}/H_2O_2, B – Fe^{3+}/H_2O_2, C – $Fe^{2+}/S_2O_8^{2-}$, D – $Fe^{3+}/S_2O_8^{2-}$, E – US/Fe^{2+}/H_2O_2, F – US/Fe^{3+}/H_2O_2, G – US/$Fe^{2+}/S_2O_8^{2-}$, H – US/$Fe^{3+}/S_2O_8^{2-}$, I – UV/Fe^{2+}/H_2O_2) in the terms of the mineralization of a model solution containing HCOONa (250 mg L^{-1} at $t = 0$) (conditions: $[Fe^{2+/3+}] = 1.25$ mmol L^{-1}, $[H_2O_2$ or $S_2O_8^{2-}]/[Fe^{2+}] = 27.5$, pH 3).

small portion of sample (1–2 mL) was taken without precipitating the iron.

2.4. Analyses

Calorimetry was used to specify the ultrasonic power dissipated into a liquid. The power was calculated by the following equation, Eq. (3) [31,32];

$$P = mC_p\left(\frac{\Delta T}{\Delta t}\right) \quad (3)$$

where m (g), C_p (J g^{-1} °C^{-1}) and $\Delta T/\Delta t$ (°C s^{-1}) denote the solution mass, the specific heat capacity (4.187 J g^{-1} °C^{-1} for water) and the rate of temperature increase, respectively. The power efficiency obtained by the ultrasonic power dissipated into a liquid divided by the input electric power was estimated at 27.9% (0.5 L) and 16.7% (0.1 L) at 20 kHz and 200 W input condition.

In order to determine the sonochemical efficiency in the whole reaction system, KI dosimetry (Weissler reaction) was employed. The method is based on the oxidation of I^- ions to I_2 due to the ultrasound irradiation. I_2 reacts with the I^- ions present in excess, giving the I_3^-, with the measurable absorbance at $\lambda_{max} = 355$ nm [33]. Sonochemical efficiency (SE) was then calculated by Eq. (4)

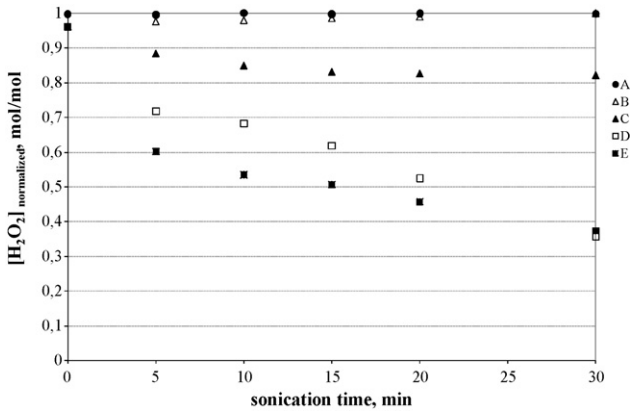

Fig. 4. Concentration of H_2O_2 vs. time during the sonication of H_2O_2 model solution; A – $[H_2O_2] = 100$ mmol L^{-1}, B – $[H_2O_2] = 20$ mmol L^{-1}, C – $[H_2O_2] = 20$ mmol L^{-1} (without temperature control), US assisted Fenton (D) and Fenton process, Fe^{2+}/H_2O_2 (E) studied in this work.

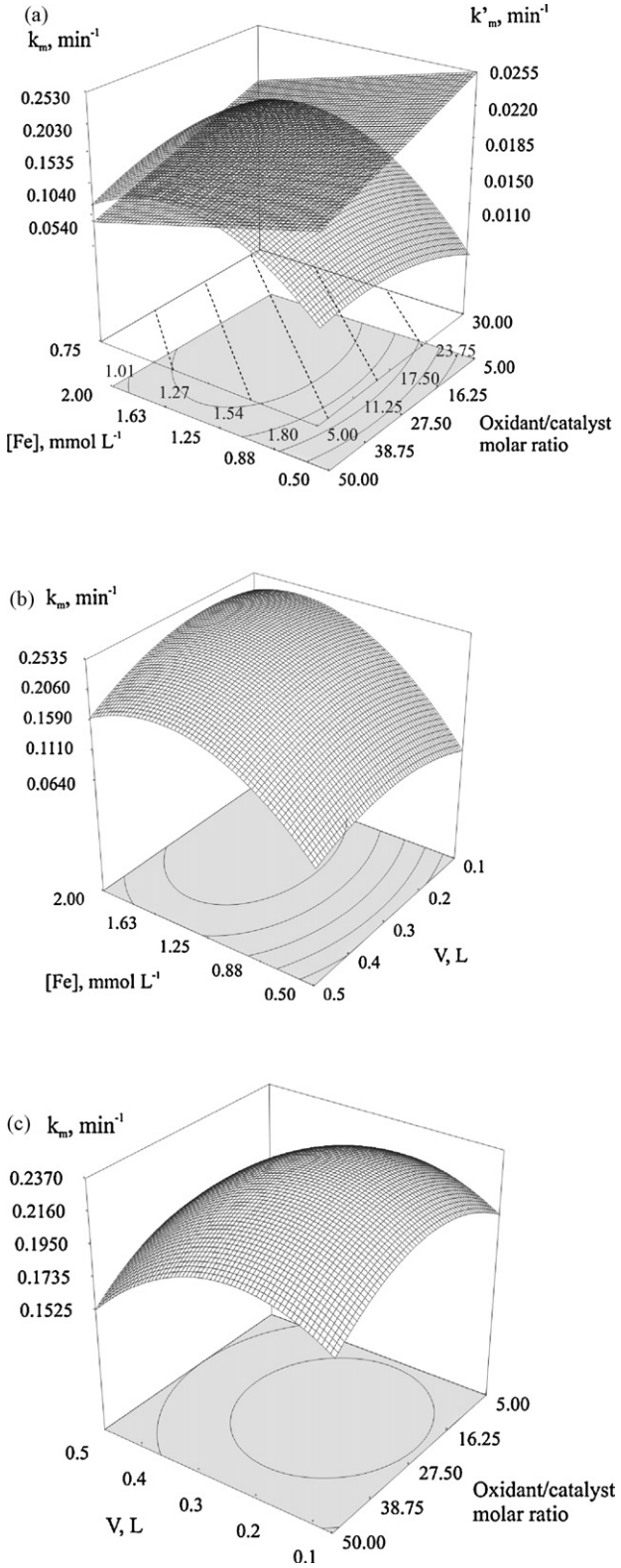

Fig. 5. Graphical interpretation of the models that describes dependency of the overall mineralization rate constant to the selected process parameters and their interactions; (a) effects of the catalyst concentration and oxidant/catalyst ratio on the performance of the US/Fe^{2+}/H_2O_2 (□ – upper base) and US/$Fe^{2+}/S_2O_8^{2-}$ (□ – lower base) processes ($V = 0.5$ L); (b) combined effects of the catalyst concentration and reaction volume ($[H_2O_2]/[Fe^{2+}] = 27.5$) and (c) combined effects of the oxidant/catalyst ratio and reaction volume on the overall mineralization rate constant achieved by US/Fe^{2+}/H_2O_2 process ($[Fe^{2+}] = 1.25$ mmol L^{-1}).

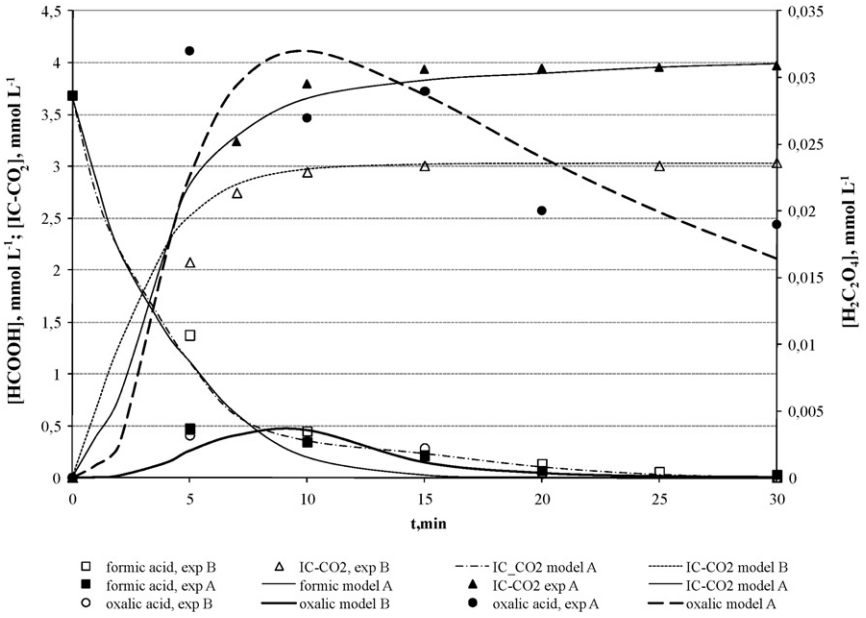

Fig. 6. Model prediction for the kinetics of the oxidation of organic compounds (formic and oxalic acid) and the mineralization (IC-CO_2) in the studied systems by US/Fe^{2+}/H_2O_2 (A) (process performed at optimal operating conditions, see cycle 3, Table 4) and US/Fe^{2+}/$S_2O_8^{2-}$ (B) ([Fe^{2+}] = 1.8 mmol L^{-1}, [$S_2O_8^{2-}$]/[Fe^{2+}] = 30) process (US: 20 kHz, 200 W nominal power).

[32,33];

$$SE = \frac{[I_3^-] \times V}{(P \times t)} \quad (4)$$

where [I_3^-] (mol L^{-1}) is the concentration of triiodide formed, V (L) is the solution volume, P (W) is the calorimetrically determined power and t (s) is the sonication time. The results of the KI dosimetry and calculated SE (mol J^{-1}) are presented in Fig. 2. Calorimetric measurements in the insulated system were repeated at least twice and the average values (in terms of SE) were reported.

Mineralization extents were determined on the basis of total organic carbon content measurements (TOC), performed by using total organic carbon analyzer; TOC-V_{CPN} 5000 A, Shimadzu. Concentration of formic and oxalic acid in supernatant were determined using High Performance Liquid Chromatographer HPLC, Shimadzu, with SUPELCOGEL H Carbohydrate column, length 250 mm, internal diameter 4.6 mm and UV detection at 210 nm. The mobile phase was 0.5% phosphoric acid with the flow rate of 0.15 mL min^{-1}.

The concentration of H_2O_2 was determined by using the procedure described in the literature [34]. The method is based on the reaction of H_2O_2 with ammonium metavanadate in acidic medium, which results in the formation of a red-orange colored peroxovanadium cation, with maximum absorbance at 450 nm and its formation was also monitored by the same UV–vis spectrophotometer. The concentration of $S_2O_8^{2-}$ ions was also determined by using the procedure described in the literature, including the reaction of $S_2O_8^{2-}$ ions with ferrous ammonium sulfate and ammonium thiocyanate and detection at 450 nm [35]. The concentration of both H_2O_2 and $S_2O_8^{2-}$ were monitored during the processes. The concentration of ferrous and ferric ions in the bulk was measured by colorimetric method using the UV–vis spectrophotometer, Lambda EZ 201, Perkin Elmer, USA. Ferrous ions were identified by the reaction of Fe^{2+} with 1,10-phenantroline giving an orange-red complex (λ_{max} = 510 nm). Ferric ions were identified by the reaction of Fe^{3+} with thiocyanate forming a red-colored complex (λ_{max} = 480 nm) under acidic conditions [36].

2.5. Experimental design

Among response surface methodology (RSM) techniques, Box–Behnken design (BBD) is commonly chosen for the purpose of a response optimization [1,37,38]. This is a three-level spherical design with excellent predictability particularly in cases when prediction of response at the extreme level is not the goal of the model. A BBD with three numeric factors; ferrous ions initial concentration (X_1), oxidant/catalyst molar ratio (X_2) and reaction volume (X_3), varied over three levels (Table 1) was used to determine the operating conditions for maximizing the organic pollutant degradation, i.e. mineralization extent in the US/Fe^{2+}/H_2O_2 process system. Since BBD was not applicable for the US/Fe^{2+}/$S_2O_8^{2-}$ process due to taking into account only two operating parameters, the three-level factorial design (3^k) was used, and two numeric factors were varied over three levels as well (Table 1). This experimental design was chosen since the volume factor has shown an insignificant effect on the mineralization extent in this particular studied system and within this particular reactor configuration and geometry. Standard arrays including combination of the selected factors and corresponding experiments are presented as a Supplementary material (Tables A.1 and A.2). The observed response was expressed as an

Table 1
Control factors in the applied processes and their levels used for the BBD and 3^2 factorial designs.

Actual factor	Code	Level		
		−1	0	1
US/Fe^{2+}/H_2O_2 process				
[Fe^{2+}] (mmol L^{-1})	X_1	0.50	1.25	2.00
Oxidant/catalyst molar ratio ([H_2O_2]/[Fe^{2+}])	X_2	5	27.50	50
Reaction volume, V (L)	X_3	0.1	0.3	0.5
US/Fe^{2+}/$S_2O_8^{2-}$ process				
[Fe^{2+}] (mmol L^{-1})	X'_1	0.75	1.27	1.80
Oxidant/catalyst molar ratio ([$S_2O_8^{2-}$]/[Fe^{2+}])	X'_2	5	17.5	30

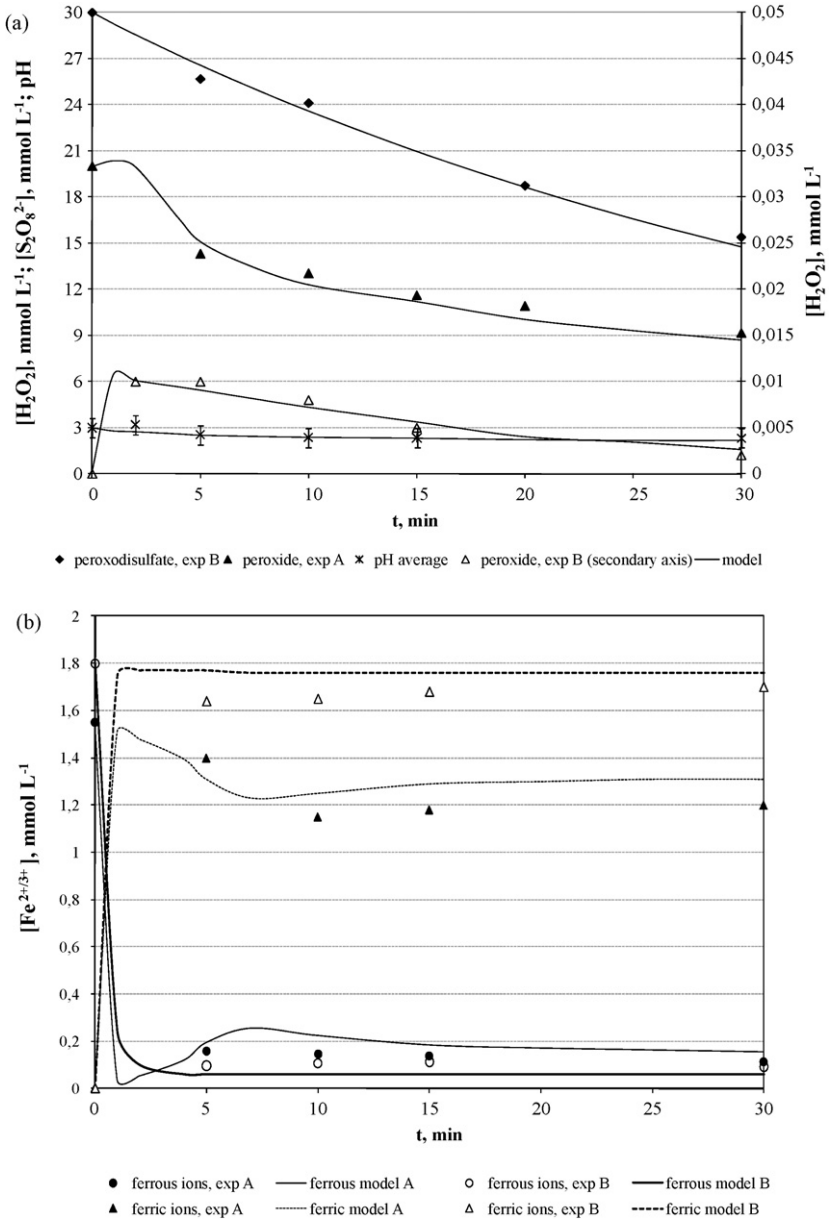

Fig. 7. Model prediction for the H_2O_2 and $S_2O_8^{2-}$ concentration, changes in pH (a) and Fe^{2+} and Fe^{3+} concentration (b) during the applied processes – US/Fe^{2+}/H_2O_2 (A) and US/Fe^{2+}/$S_2O_8^{2-}$ (B).

overall mineralization rate constant. Obtained models and experimental data were analyzed statistically using *Design-Expert 6.0.6*, a DoE software tool from Stat-Ease, Inc.

The control factors and their values were determined based on prior experiences [1]. The desirability function approach (DFA) was utilized for the single-response optimization [1], to determine how input parameters affect the desirability of individual response.

3. Results and discussion

3.1. Preliminary studies

As shown in Fig. 3, mineralization achieved within the studied processes was expressed as conversion of organic species present in the system to the inorganic products, Eq. (5). The initial TOC value of approximately 45 mg L^{-1} has been attributed to the 250 mg L^{-1} of sodium formate.

$$X_m(t) = \frac{TOC_{initial} - TOC(t)}{TOC_{initial}} \quad (5)$$

When making comparison between those processes, it is obvious that employment of ultrasound enhanced the conversion, even within the first 5 min of sonication. The beneficial effect of the ultrasonic energy on the performance of Fenton and Fenton-like processes was already reported [3,11,39–42]. Obviously, the degradation in US/Fenton system is rapid. As it can be seen from Fig. 3, the mineralization extent of approximately 81% could be obtained by classic Fenton process, Fe^{2+}/H_2O_2, after 30 min of reaction, but after only 5 min by applying the ultrasound (US/Fe^{2+}/H_2O_2). This can be explained by the fact that sonication of the system allows a better homogenization and more effective mass transfer that could be compared with well-mixing. Furthermore, US waves induce a cavitation, i.e. formation of a bubble and its consequent collapse leaving in the system a large amount of energy [21,43]. Outside the

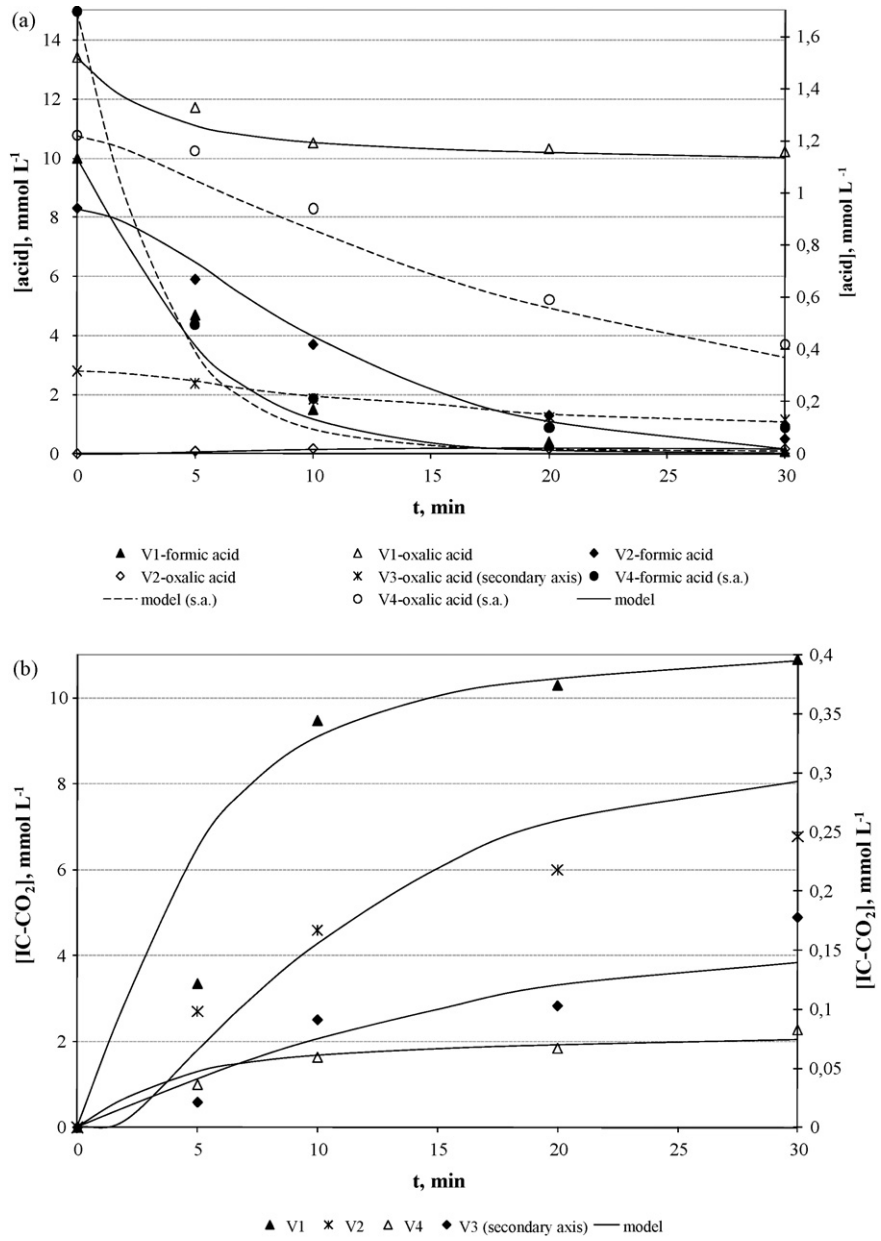

Fig. 8. Validation of the developed models for the applied processes; formic and oxalic acid oxidation kinetics (a) and mineralization kinetics (b). Conditions were given in Table 7.

bubble, water molecules are readily decomposed and radicals are formed [11] (Eq. (6)).

$$H_2O \xrightarrow{)))} H^{\bullet} + {}^{\bullet}OH \quad (6)$$

When comparing the efficiency of an UV and US assisted Fenton processes (Fig. 3), some conclusion could be drawn. The overall conversion in terms of the mineralization of the system is almost the same in both cases. In order to shorten the treatment time and to reduce the amount of the Fenton reagent needed UV light is introduced in the systems treated by Fenton-like processes, with a special emphasis on a heterogeneous ones [44–50]. Furthermore, sonication could results with the same positive effect [42]. When observing Eqs. (7)–(11) [51],

$$Fe^{3+} + H_2O \rightarrow [Fe(OH)]^{2+} + H^+ \quad (7)$$

$$[Fe(OH)]^{2+} \xrightarrow[\text{or })))]{h\nu} Fe^{2+} + {}^{\bullet}OH \quad (8)$$

$$Fe^{3+} + H_2O_2 \rightarrow Fe(OOH)^{2+} + H^+ \quad (9)$$

$$Fe(OOH)^{2+} \xrightarrow{)))} Fe^{2+} + HO_2{}^{\bullet} \quad (10)$$

$$Fe^{2+} + H_2O_2 \rightarrow Fe^{3+} + OH^- + {}^{\bullet}OH \quad (11)$$

it is obvious that both UV irradiation and ultrasonic waves favorize the formation of hydroxyl radicals within the frame of the Fenton cycle. Thus, both type of energy employment could be utilized to enhance the Fenton process yielding in terms of mineralization of the wastewater systems loaded with different organic pollutants. The beneficial effect of the US could also be observed on Fig. 3. Namely, only 32% of mineralization was achieved by the Fe^{3+}/H_2O_2 process, while the obtained extent of 68% was observed when US was applied. This enhancement could be attributed to the formation of $^{\bullet}OH$ and releasing of the catalytic Fe^{2+} ions described by Eqs. (8) and (10).

The other idea presented in the current study, was to change an oxidant in the Fenton cycle in order to examine a potential

conversion in terms of mineralization in the system. In the case where some particular amounts of sulfate ions lapsed in the system treated by $S_2O_8^{2-}$ have a small or even negligible influence on the quality of the treated system, by utilizing persulfate salt it is possible to overcome disadvantages referred to the usage of H_2O_2, i.e. reagent instability, storage and handling issues. Persulfate anions, $S_2O_8^{2-}$, were chosen as an alternative oxidant due to possibility for a consequent generation of different nonselective radicals, $^{\bullet}OH$, $S_2O_8^{\bullet-}$ and $SO_4^{\bullet-}$, Eqs. (12)–(15) [11,17,52].

$$Fe^{2+} + S_2O_8^{2-} \rightarrow Fe^{2+} + SO_4^{\bullet-} + SO_4^{2-} \quad (12)$$

$$SO_4^{2-} + {}^{\bullet}OH \rightarrow SO_4^{\bullet-} + OH^- \quad (13)$$

$$S_2O_8^{2-} + {}^{\bullet}OH \rightarrow S_2O_8^{\bullet-} + OH^- \quad (14)$$

$$SO_4^{\bullet-} + H_2O \rightarrow SO_4^{2-} + {}^{\bullet}OH + H^+ \quad (15)$$

The additional amount of sulfate radicals is formed during sonication, Eq. (16) [25]

$$S_2O_8^{2-} \xrightarrow{)))} 2SO_4^{\bullet-} \quad (16)$$

In all the sonicated systems, a small portion of H_2O_2 is generated due to a recombination of a free radicals formed after the bubble collapse [11,40]. Nevertheless, a rapid consumption of H_2O_2 in the Fenton catalytic cycle has also been observed when US was employed (Fig. 4), implying on the insignificant influence of the in situ generation of H_2O_2 on the mineralization efficiency. The results obtained for the test experiments where only model solution of H_2O_2 was sonicated, showed the following; the almost unchanged (steady-state) concentration of H_2O_2 with time (i) and H_2O_2 decomposition due to the generated heat (ii). Steady-state concentration of H_2O_2 in a controlled system can be explained by the parallel reactions of H_2O_2 formation due to cavitational activity, Eqs. (6) and (17)–(20), and its sonolysis, Eq. (21) [53].

$$2{}^{\bullet}OH \rightarrow H_2O_2 \quad (17)$$

$$H^{\bullet} + {}^{\bullet}OH \rightarrow H_2O_2 \quad (18)$$

$$H^{\bullet} + O_2 \rightarrow HO_2^{\bullet} \quad (19)$$

$$2{}^{\bullet}OH \rightarrow H_2O + 1/2\,O_2 \quad (20)$$

$$H_2O_2 \xrightarrow{)))} 2{}^{\bullet}OH \quad (21)$$

Table 2
RSM model equations for the observed responses.

Response	Equation
US/Fe^{2+}/H_2O_2 process	
k_m (min^{-1})	$-0.24498 + 0.47413$ $[Fe^{2+}] + 4.39221 \times 10^{-3}$ $([H_2O_2]/[Fe^{2+}]) + 5.61492 \times 10^{-4}$ $V - 0.12748$ $[Fe^{2+}]^2 - 5.39358 \times 10^{-5}$ $([H_2O_2]/[Fe^{2+}])^2 - 8.48250 \times 10^{-7}$ $V^2 - 1.37481 \times 10^{-3}$ $[Fe^{2+}] \cdot ([H_2O_2]/[Fe^{2+}]) - 1.01833 \times 10^{-4}$ $[Fe]\,V$
US/Fe^{2+}/$S_2O_8^{2-}$ process	
k'_m (min^{-1})	$4.78170 \times 10^{-3} + 6.42921 \times 10^{-3}$ $[Fe^{2+}] + 3.07907 \times 10^{-4}$ $([H_2O_2]/[Fe^{2+}])$

3.2. Statistical analysis, optimization and interpretation

The statistical study of the studied processes; US/Fe^{2+}/H_2O_2 and US/Fe^{2+}/$S_2O_8^{2-}$, was performed using response surface methodology BBD and 3^2 factorial design (Supplementary material, Tables A.1 and A.2). Individual parameters and their interaction effects on mineralization kinetics, expressed as the overall mineralization rate constants according to the pseudo-first-order reaction kinetics, were determined and statistical models of process were developed (Table 2.). The presented model equations, given in the terms of the actual factors, showed the strong dependency of a mineralization rate on the Fenton reagent dosage while the reaction volume had an insignificant effect on the mineralization extent in this particular studied system and within this particular reactor configuration and geometry.

For current study response surface models were evaluated using ANOVA. *F*-values of 51.75 and 15.26 and *p*-values less than 0.05 imply that the model is significant. Significant terms in each predictive model, with the *p*-value less than 0.1000 are given as well (Table 3). The dependency of the mineralization kinetics on the set of operating parameter is shown on Fig. 5.

As it can be seen from Fig. 5, the influence of the reaction volume on mineralization kinetics as an indirect approximate measure of the sonication power has no significant influence within the investigated range. Since, the slightly better mineralization extent was achieved in the middle of the investigated range, the

Table 3
ANOVA results—model and coefficient validation; fit summary.

Source	Sum of squares	Mean square	Degrees of freedom	*F*-value	*p*-Value	R^2
US/Fe^{2+}/H_2O_2 process (BBD)						
Model	0.072	8.957×10^{-3}	8	51.75	<0.0001	0.9810
X_1	0.034	0.034	1	197.17	<0.0001	
X_2	3.470×10^{-4}	3.470×10^{-4}	1	2.01	0.1944	
X_3	1.788×10^{-3}	1.788×10^{-3}	1	10.33	0.0123	
X_1^2	0.022	0.022	1	125.08	<0.0001	
X_2^2	3.139×10^{-3}	3.139×10^{-3}	1	18.14	0.0028	
X_3^2	4.847×10^{-3}	4.847×10^{-3}	1	28.01	0.0007	
X_1X_2	2.153×10^{-3}	2.153×10^{-3}	1	12.44	0.0078	
X_1X_3	9.330×10^{-4}	9.330×10^{-4}	1	5.39	0.0488	
Total	0.073	–	16	–	–	
*Residual error*Lack-of-fit	1.036×10^{-3}	2.590×10^{-4}	4	2.97	0.1584	
US/Fe^{2+}/$S_2O_8^{2-}$ process (3^2 factorial design)						
Model	1.572×10^{-4}	7.862×10^{-5}	2	15.26	0.0009	0.9275
X'_1	6.836×10^{-5}	6.836×10^{-5}	1	13.27	0.0045	
X'_2	8.888×10^{-5}	8.888×10^{-5}	1	17.25	0.0020	
Total	2.088×10^{-4}	–	12	–	–	
*Residual error*Lack-of-fit	3.178×10^{-5}	5.296×10^{-6}	6		0.4958	

Table 4
Single-response optimization of US/Fe^{2+}/H_2O_2 process via DFA and results.

Optimization cycle	Objective	Criteria	Result	Desirability of the result (d) (%)	Predicted value
1.		$[Fe^{2+}] \leq 1$ mmol L^{-1} $5 < [H_2O_2]/[Fe^{2+}] < 30$ $V \Rightarrow$ maximum (0.5 L)	$[Fe^{2+}] = 1.14$ mmol L^{-1} $[H_2O_2]/[Fe^{2+}] = 27.5$ $V = 0.5$ L	71.0	$k_m = 0.1777$ min^{-1}
2.	$k_m \Rightarrow$ maximum	$[Fe^{2+}] \leq 2$ mmol L^{-1} $[H_2O_2]/[Fe^{2+}] \Rightarrow$ minimum $V \Rightarrow$ maximum (0.5 L)	$[Fe^{2+}] = 1.86$ mmol L^{-1} $[H_2O_2]/[Fe^{2+}] = 5$ $V = 0.5$ L	80.6	$k_m = 0.1775$ min^{-1}
3.		$[Fe^{2+}] \leq 2$ mmol L^{-1} $5 < [H_2O_2]/[Fe^{2+}] < 20$ $V \Rightarrow$ maximum (0.5 L)	$[Fe^{2+}] = 1.55$ mmol L^{-1} $[H_2O_2]/[Fe^{2+}] = 20$ $V = 0.5$ L	75.5	$k_m = 0.1971$ min^{-1}

Table 5
The reactions and rate constants used for the kinetic modeling; based on a mechanistic model and a homogeneous reaction system.

No.	Reaction	Rate constant (L mol^{-1} min^{-1})
Formic and oxalic acid oxidation pathway		
Initiated by radicals		
R1	$HCOOH + OH^\bullet \rightarrow CO_2^{\bullet-} + H_2O + H^+$	8.4×10^9 [19]
R2	$CO_2^{\bullet-} + CO_2^{\bullet-} \leftrightarrow [CO_2^{\bullet-}\cdots CO_2^{\bullet-}]$	$K_{eq} = 1 \times 10^4$ L mol^{-1}
R3	$[CO_2^{\bullet-}\cdots CO_2^{\bullet-}] \rightarrow C_2O_4^{2-}$	2.4×10^9 min^{-1} [20]
R4	$[CO_2^{\bullet-}\cdots CO_2^{\bullet-}] \rightarrow 2CO_2$	3×10^9 min^{-1}
R5[a]	$(1-\alpha)H_2C_2O_4 + 2OH^\bullet \rightarrow (CO_2)_2^{\bullet-} + 2OH^-$	1.8×10^8
R6	$(1-\alpha)\ H_2C_2O_4 + SO_4^{\bullet-} \rightarrow (CO_2)_2^{\bullet-} + SO_4^{2-}$	8.4×10^7
R7	$(CO_2)_2^{\bullet-} + (CO_2)_2^{\bullet-} \leftrightarrow [(CO_2)_2^{-}\cdots(CO_2)_2^{-}]$	$K_{eq} = 1 \times 10^4$ L mol^{-1}
R8	$[(CO_2)_2^{-}\cdots(CO_2)_2^{-}] \rightarrow 2CO_2 + C_2O_4^{2-}$	4.62×10^8 min^{-1} [20]
R9	$(CO_2)_2^{\bullet-} \rightarrow CO_2^{\bullet-} + CO_2$	1×10^{11}
Sonolysis		
R10	$HCOOH \xrightarrow{)))} CO_2 + 2H^+$	1.76×10^{-7} min^{-1} [21]
R11	$(1-\alpha)H_2C_2O_4 \xrightarrow{)))} 2CO_2 + H_2O$	3.16×10^{-8} min^{-1}
Enhancement of a Fenton catalytic cycle		
R12	$Fe(OH)^{2+} \xrightarrow{)))} Fe^{2+} + OH^\bullet$	300 min^{-1}
R13	$Fe(OOH)^{2+} \xrightarrow{)))} Fe^{2+} + OH_2^\bullet$	600 min^{-1}
Reaction scheme previously established [11,22–26]		
Fenton catalytic cycle		
R14	$Fe^{2+} + H_2O_2 \rightarrow Fe^{3+} + OH^\bullet$	4560
R15	$Fe^{3+} + H_2O_2 \rightarrow Fe(OOH)^{2+} + H^+$	0.6
R16	$Fe^{2+} + OH^\bullet \rightarrow Fe^{3+} + OH^-$	1.92×10^{10}
R17	$Fe^{2+} + HO_2^\bullet \rightarrow Fe^{3+} + H_2O_2$	7.2×10^7
R18	$Fe^{3+} + HO_2^\bullet \rightarrow Fe^{2+} + H^+ + O_2$	1.86×10^7
R19	$Fe^{3+} + O_2^{\bullet-} \rightarrow Fe^{2+} + O_2$	3×10^9
R20	$Fe^{2+} + O_2^{\bullet-} \rightarrow Fe^{3+} + H_2O_2$	6×10^8
R21	$Fe^{2+} + S_2O_8^{2-} \rightarrow Fe^{3+} + SO_4^{\bullet-} + SO_4^{2-}$	39
R22	$Fe^{3+} + S_2O_8^{2-} \rightarrow Fe^{2+} + 2SO_4^{\bullet-}$	29.5
R23	$Fe^{2+} + SO_4^{\bullet-} \rightarrow Fe^{3+} + SO_4^{2-}$	1×10^6
Complexes formation		
R24	$Fe^{3+} + H_2O \rightarrow [Fe(OH)]^{2+} + H^+$	1.86×10^{-3}
R25[a]	$Fe^{3+} + \alpha$ oxalic acid $\rightarrow$ Fe-oxalate complexes	60
Liquid-phase reactions		
R26	$OH^\bullet + H_2O_2 \rightarrow HO_2^\bullet + H_2O$	7.2×10^8
R27	$2OH^\bullet \rightarrow H_2O_2$	3.18×10^{11}
R28-1	$H_2O_2 \rightarrow HO_2^- + H+$	2.22
R28-2	$HO_2^- + H+ \rightarrow H_2O_2$	1.56×10^{12}
R29	$OH^\bullet + HO_2^- \rightarrow HO_2^\bullet + H_2O$	4.5×10^{11}
R30	$OH^\bullet + HO_2^\bullet \rightarrow H_2O + O_2$	3.96×10^{11}
R31	$2HO_2^\bullet \rightarrow H_2O_2 + O_2$	4.98×10^7
R32	$HO_2^\bullet \rightarrow O_2^{\bullet-} + H^+$	9.48×10^6 min^{-1}
R33	$OH^\bullet + H_2O_2 \rightarrow O_2^{\bullet-} + H_2O$	1.62×10^9
R34	$HO_2^\bullet + O_2^{\bullet-} \rightarrow HO_2^- + O_2$	5.82×10^9
R35	$OH^\bullet + O_2^{\bullet-} \rightarrow O_2 + OH^-$	4.2×10^{11}
R36	$O_2^{\bullet-} + H^+ \rightarrow HO_2^\bullet$	6×10^{11}
R37	$SO_4^{\bullet-} + H_2O \rightarrow HO^\bullet + H^+ + SO_4^{2-}$	6.3×10^7
R38	$SO_4^{2-} + {}^\bullet OH \rightarrow SO_4^{\bullet-} + OH^-$	1.18×10^6 [16]
Ultrasonic induced radical formation		
R39	$H_2O \xrightarrow{)))} H^\bullet + OH^\bullet$	2×10^{-5} min^{-1}
R40	$H^\bullet + O_2 \rightarrow HO_2^\bullet$	1×10^{11}
R41	$H_2O_2 \xrightarrow{)))} 2OH^\bullet$	0.7 min^{-1}
R42	$S_2O_8^{2-} \xrightarrow{)))} 2SO_4^{\bullet-}$	5×10^2 min^{-1}

[a] Part of oxalic acid that involves in complexation with Fe^{3+} is set at 20%, i.e. $\alpha = 0.2$.

following could be concluded; (i) when the reaction volume is rather small, ultrasonic waves are spread easily and the sonication power at each point within the reaction space is almost the same and relatively high, (ii) in a larger volume, as the waves are spreading from the center to the walls of the reactor, passing through a bigger reaction space, the dissipation of the sonication power comes to an issue, and (iii) there is a temperature optimum for the sonochemical processes, and a sonication power in the system should not be increased in a manner that distorts that optimum. Additionally, the results of the KI dosimetry performed in different reaction volumes (Fig. 2), showed the similar I_3^- yields, but the higher value of the sonochemical efficiency in the larger reaction volume (0.5 L). The given statements can be also confirmed by the temperature observation with the sonication time. In smaller reaction volume (<100 mL), the temperature tends to rise rapidly (>3 °C/min) in comparison with the approximately 1–1.5 °C/min temperature increase observed for the larger reaction volume (0.5 L). The observed difference in the temperature increase can be attributed to the more pronounced cavitation activity throughout the reaction space. However, the more extensive bubble collapse and more energy released at a single point of the reaction space do not guarantee the enhanced efficiency of the sonochemical wastewater treatment, as the ongoing reaction rates have certain temperature dependence. For example, it is well known fact that in order to avoid precipitation of iron hydroxide, simultaneous high reaction temperature (>55 °C) and iron concentration (>9 ppm) should be prevented [54]. Also, H_2O_2 decomposition rate is increasing rapidly at higher temperatures (Fig. 4) [55]. With this in mind, and including the fact that the intention explored within this work is to process the oxidation with more than 1 mmol L^{-1} (56 ppm) of iron ions, but at lower H_2O_2 concentration, rapid temperature increase should be avoided. In the frame of this work, it was ensured by intensive cooling throughout the water jacket (Fig. 1) and by performing the further experiments in the larger reaction volume. The further discussion about the complexity of the cavitation phenomena and temperature optimum for sono-Fenton performance was given in our previous work [11].

Optimization of a single response, i.e. overall mineralization rate constant, was performed including the determination of the influence of the input parameters on the desirability of the particular individual response. An optimal design point was achieved by adjusting the settings for input parameters (criteria) while overall mineralization rate constant was kept at maximum. Desired settings for input parameters, i.e. criteria are presented in Table 4 along with the results for an optimal design point for the US/Fe^{2+}/H_2O_2 and its desirability according to the set criteria. Optimization was performed in three cycles, changing the criteria adjustments (Table 4). For further investigation the third cycle from Table 4 was chosen ($[Fe^{2+}] = 1.55$ mmol L^{-1}, $[H_2O_2]/[Fe^{2+}] = 20$). As far as concern US/Fe^{2+}/$S_2O_8^{2-}$ process, optimization was performed without setting the criteria for the input parameters; only the mineralization rate was kept at maximum. The established optimal conditions were as follows; $[Fe^{2+}] = 1.8$ mmol L^{-1}, $[S_2O_8^{2-}]/[Fe^{2+}] = 30$. For the both processes, the reaction volume was set at 0.5 L.

When comparing the results obtained for the US/Fe^{2+}/H_2O_2 (Table 4) and processes (Fig. 3a), it can be seen that the initial concentration of ferrous ions (X_1) has the highest influence on the overall efficiency of the US/Fe^{2+}/H_2O_2 process, while the oxidant/catalyst ratio (X_2') is crucial for the US/Fe^{2+}/$S_2O_8^{2-}$ process performance. It can be explained by the yielding of the persulfate/Fenton cycle due to a minor activity of $S_2O_8^{\bullet-}$ and $SO_4^{\bullet-}$ compared to a hydroxyl radical. Since in that particular system, these radical are predominate to the $^{\bullet}OH$, the larger amount of persulfate is needed to achieve the sufficient yield in terms of a free radical generation.

3.3. Development of a mathematical model

All the observed phenomena in the study could be described by a mathematical model developed according to a mechanistic scheme. All the reactions involved in the model development were given in a Table 5, along with the corresponding rate constants and literature references. The formate ions as well as a formic acid, present initially in the system (at a given pH, the molar ratio of formic acid and formate ions is approximately 57 in a favour of the acid according to the dissociation equilibrium), can be attacked by a free radical giving the carboxyl radical, $CO_2^{\bullet-}$, (R1, Table 5) [19]. The generated $CO_2^{\bullet-}$ radical is present in this form throughout most of the pH range and only protonated ($HCO_2^{\bullet}$) in strongly acidic solution (pH < 2). It is suggested that an intermediate of the cage recombination of these radicals, $[CO_2^{\bullet-}\cdots CO_2^{\bullet-}]$ is produced in the next step (R2) [20]. This intermediate can further lead to the formation of stable products such as oxalate/oxalic acid (R3) and CO_2 (R4) or dissociate back to $CO_2^{\bullet-}$ radicals (R2 – equilibrium) [1,28]. A considerable amount of oxalic acid (above the HPLC detection level) was observed during the experiments (Fig. 6). Its formation and a consequent degradation were monitored with the reaction time. The fate of the oxalic acid/oxalate anions has a similar pathway under the radical attack (R5–R8) [20,56]. In the first step dicarboxyl radical $(CO_2)_2^{\bullet-}$, is formed. Following reactions involve a cage recombination of those radicals, yielding with CO_2 and oxalate anion (R8). Again, at the given pH, dissociation equilibrium goes in favour of oxalic acid over its anions in the studied system. It is important to point out that the reaction of formic acid towards carboxyl radicals is induced only by hydroxyl radicals. The oxidation pathway of formic acid by hydroxyl radical is predominant in comparison with the sulfate radicals. On the other hand, somewhat slower reaction between oxalic acid and hydroxyl radicals, allows the existence of an oxidation pathway initiated by sulfate radicals (R6). Degradation of formate and oxalate species by secondary mechanisms, i.e. pyrolysis in the cavitation bubble and supercritical water oxidation at the liquid-bubble interphase, was considered as negligible due to the hydrophilic properties and relatively low vapor pressure of the formic and oxalic acid, as well as the low concentration in the system [57] (R10 and R11).

The other reactions accounted for the model development were reported earlier [11], including the Fenton catalytic cycle, free radical reactions and ultrasonic induced reactions [22–26] (Table 5). A homogeneous reaction system was assumed. Regarding the general mass balance for a well-mixed, constant volume and constant temperature batch reactor given by Eq. (22),

$$r_i = \frac{dc_i}{dt} \tag{22}$$

where c_i is concentration of specie i in the bulk and r_i is the bulk phase rate of the same specie; mineralization of a model wastewater in terms of formic acid degradation and axalic acid generation and a consequent degradation was simulated by Mathematica 7.0 (Wolfram Research) using GEAR method (backward differentiation) to find the numerical solution to the set of ordinary differential equations.

Values of the rate constants for the following reactions; R4–R6, R8, R12, R13, as well as the constants for the equilibrium between the carboxyl and dicarboxyl radicals and their cage recombination intermediates (R2 and R7) (Table 5) were determined by trial and error method fitting the experimental values into the model (Figs. 6 and 7). Accuracy of developed model for the each system was evaluated by the mean of the normalized root mean square deviation (NRMSD) [11,58] as shown in Table 6. NRMSDs

Table 6
Normalized root mean square deviation (NRMSD) calculations for the evaluation of model accuracy.

NRMSDs	Process	
Observed value	US/Fe^{2+}/H_2O_2	US/Fe^{2+}/$S_2O_8^{2-}$
[Formic acid]	0.0424	0.0906
[Oxalic acid]	0.1693	0.0010
[IC-CO_2]	0.0566	0.0278
[H_2O_2]	0.0131	0.0739
[$S_2O_8^{2-}$]	–	0.0082
[Fe^{2+}]	0.0184	0.0384
[Fe^{3+}]	0.0234	0.0225
pH	0.0628	0.0475

obtained for the monitored values; concentration of formic and oxalic acid, difference for the TOC content an a system, H_2O_2 and $S_2O_8^{2-}$ concentration, pH, ferrous and ferric ions concentration, are around 0.05, indicating the good match between the observed values and the ones predicted by the model. It can be also stated that the assumed reactions of the Fenton catalytic cycle and reactions involving the US implication are confirmed owing to these observations.

In order to validate the developed model, an additional set of experiments has been performed (V1–V4, Table 7). The model solutions consisting of the higher initial concentration of the HCOONa (i), a mixture of the HCOONa and oxalic acid (ii) and a model solution consisted of the oxalic acid only, were treated by the studied processes, US/Fe^{2+}/H_2O_2 and US/Fe^{2+}/$S_2O_8^{2-}$. Model solutions were chosen carefully to examine the validity of the model in the case of the different initial organic loadings and acid compositions. The specific conditions for each validation experiment are stated in Table 7. These conditions (V1, V3 and V4) were set specifically to explore the application of the developed model outside the previously set design space. Only experiment V2 was performed at the established optimal conditions for the US/Fe^{2+}/H_2O_2 process. The results showed the good match with the model simulations, as shown in Fig. 8 and Table 7 (NRMSD values), thus confirming the models validity and applicability.

Table 7
Validation of the developed models for US/Fe^{2+}/H_2O_2 and US/Fe^{2+}/$S_2O_8^{2-}$ processes.

Description	NRMSDs		
	[Formic acid]	[Oxalic acid]	[IC-CO_2]
V1			
US/Fe^{2+}/H_2O_2			
[Fe^{2+}] = 3.75 mmol L^{-1}			
[H_2O_2] = 80 mmol L^{-1}			
Model solution:	0.0224	0.0096	0.0583
$TOC_{initial}$ = 275 mg L^{-1}			
w(HCOONa) = 3/7			
w($H_2C_2O_4$) = 4/7			
V2			
US/Fe^{2+}/H_2O_2			
[Fe^{2+}] = 1.55 mmol L^{-1}			
[H_2O_2] = 20 mmol L^{-1}	0.0173	0.0010	0.0504
Model solution (HCOONa only):			
$TOC_{initial}$ = 100 mg L^{-1}			
V3			
US/Fe^{2+}/$S_2O_8^{2-}$			
[Fe^{2+}] = 3 mmol L^{-1}			
[H_2O_2] = 50 mmol L^{-1}	0.0012	0.0124	0.0732
Model solution ($H_2C_2O_4$ only):			
$TOC_{initial}$ = 7.5 mg L^{-1}			
V4			
US/Fe^{2+}/$S_2O_8^{2-}$			
[Fe^{2+}] = 3.75 mmol L^{-1}			
[H_2O_2] = 80 mmol L^{-1}			
Model solution:	0.0190	0.0103	0.0556
$TOC_{initial}$ = 50 mg L^{-1}			
w(HCOONa) = 3/7			
w($H_2C_2O_4$) = 4/7			

4. Conclusion

The scope of this study was to evaluate the application of sonochemical AOPs; ultrasonic (US) assisted Fenton process, US/Fe^{2+}/H_2O_2, and US assisted modified Fenton process, US/Fe^{2+}/$S_2O_8^{2-}$ for the treatment of model wastewaters containing formate ions/formic acid. Preliminary results emphasised the beneficial effect of the US; e.g. the reduction of time needed to achieve mineralization in a considerable extent. It is reasonable to expect a mineralization extent of 94%, corresponding to the complete degradation of formate species with the consequent formation and the degradation of oxalic acid in the system.

To establish the effects of the operating parameters and to optimize the mineralization rate observed within the applied process in the terms of reagents consumption and an involved energy, i.e. ultrasonic power, corresponding to the treated volume, the statistical study of formate degradation was performed applying Box–Behnken experimental design for US/Fe^{2+}/H_2O_2 process, and 3 level factorial design for US/Fe^{2+}/$S_2O_8^{2-}$ process. Predictive models were developed and the effect of each parameter determined, pointing on the major effect of the catalyst concentration [Fe^{2+}] in the US/Fe^{2+}/H_2O_2 process, and a great influence of the oxidant amount [$S_2O_8^{2-}$] regarding the US/Fe^{2+}/$S_2O_8^{2-}$ process. Investigation of the influence of a reaction volume on the overall mineralization kinetics raised an issue of the sonication performance regarding the reaction temperature and the transposition of the ultrasonic waves. Furthermore, single-response optimization was attempted through desirability function based on the developed predictive models.

The detailed mathematical model describing the ongoing process in the studies batch system was developed on the basis of a mechanistic reaction scheme, taking into account free radical mechanism of formic acid degradation over carboxyl radical towards oxalic acid and CO_2. Developed mathematical model has been successfully validated, thus confirming the model applicability and accuracy in the assumptions made regarding the reaction scheme.

Moreover, US assisted Fenton process compared with the UV assisted Fenton process, UV/Fe^{2+}/H_2O_2, showed the possibility for an eventual consideration for the replacement of UV light sources with the ultrasonic technology on a larger scale.

Acknowledgments

Purchase of equipment used in this work was financially supported by The National Foundation for Science, Higher Education and Technological Development of the Republic of Croatia, in the frame of the Project #04/14, *Wastewater Treatment in DINA-Petrokemija Omišalj as a Contribution to Ecosystem Preservation*. We would also like to acknowledge the financial support from the Croatian Ministry of Science, Education and Sport, Project #125-1253092-1981.

The authors would like to express special gratitude to MSc Vesna Gržetić, chief librarian and Aleksandra Krznarić, Faculty of Chemical Engineering and Technology, Zagreb, Croatia, for an extensive help in providing the references and the supporting data.

Appendix A. Supplementary data

Supplementary data associated with this article can be found, in the online version, at doi:10.1016/j.cej.2010.08.059.

References

[1] I. Grčić, D. Vujević, J. Šepčić, N. Koprivanac, Minimization of organic content in simulated industrial wastewater by Fenton type processes: a case study, J. Hazard. Mater. 170 (2009) 954–961.
[2] R. Andreozzi, V. Caprio, A. Insola, R. Marotta, Advanced oxidation processes (AOP) for water purification and recovery, Catal. Today 53 (1999) 51–59.
[3] P.R. Gogate, Treatment of wastewater streams containing phenolic compounds using hybrid techniques based on cavitation: a review of the current status and the way forward, Ultrason. Sonochem. 15 (2008) 1–15.
[4] Y.G. Adewuyi, Sonochemistry: environmental science and engineering applications, Ind. Eng. Chem. Res. 40 (2001) 4681–4715.
[5] F. Chemat, P.G.M. Teunissen, S. Chemat, P.V. Bartels, Sono-oxidation treatment of humic substances in drinking water, Ultrason. Sonochem. 8 (2001) 247–250.
[6] J. Lin, C. Chang, J. Wu, Enhancement of decomposition of 2-chlorophenol with ultrasound/H_2O_2 process, Water Sci. Technol. 34 (1996) 75–81.
[7] L.K. Weavers, F.H. Ling, M.R. Hoffman, The combination of sonolysis and ozonolysis for aromatic compound degradation, Environ. Sci. Technol. 32 (1998) 2727–2733.
[8] F. Trabelsi, H. Ait-Lyazidi, B. Ratsimba, A.M. Wilhelm, H. Delmas, P.L. Fabre, J. Berlan, Oxidation of phenol in wastewater by sonoelectrochemistry, Chem. Eng. Sci. 51 (1996) 1857–1865.
[9] E. Manousaki, E. Psillakis, N. Kalogerakis, D. Mantzavinos, Degradation of sodium dodecylbenzene sulfonate in water by ultrasonic irradiation, Water Res. 38 (2004) 3751–3759.
[10] Z. Guo, Z. Zheng, S. Zheng, W. Hu, R. Feng, Effect of various sono-oxidation parameters on the removal of aqueous 2, 4-dinitrophenol, Ultrason. Sonochem. 12 (2005) 461–465.
[11] I. Grčić, D. Vujević, N. Koprivanac, Modeling the mineralization and discoloration in colored systems by (US)$Fe^{2+}/H_2O_2/S_2O_8^{2-}$ processes; a proposed degradation pathway, Chem. Eng. J. 157 (2010) 35–44.
[12] S.M. Rodriguez, J.B. Galvez, M.I.M. Rubio, P.F. Ibanez, W. Gernjak, I.O. Alberola, Treatment of chlorinated solvents by TiO_2 photocatalysis and photo-Fenton: influence of operating conditions in a solar pilot plant, Chemosphere 58 (2005) 391–398.
[13] J. Wang, T. Ma, Z. Zhang, X. Zhang, Y. Jiang, D. Dong, P. Zhang, Y. Li, Investigation on the sonolytic degradation of parathion in the presence of nanometer rutile titanium dioxide (TiO_2) catalyst, J. Hazard. Mater. 137 (2006) 972–980.
[14] E.V. Rokhina, M. Lahtinen, M.C.M. Nolte, J. Virkutyte, The influence of ultrasound on the RuI_3-catalyzed oxidation of phenol: catalyst study and experimental design, Appl. Catal. B: Environ. 87 (2009) 162–170.
[15] D. Drijvers, H. Van Langenhove, M. Beckers, Decomposition of phenol and trichloroethylene by the ultrasound/H_2O_2/CuO process, Water Res. 33 (1999) 1187–1194.
[16] M.G. Antoniou, A.A. de la Cruz, D.D. Dionysiou, Degradation of microcystin-LR using sulfate radicals generated through photolysis, thermolysis and e-transfer mechanisms, Appl. Catal. B: Environ. 96 (2010) 290–298.
[17] G.P. Anipsitakis, D.D. Dionysiou, Radical Generation by the Interaction of Transition Metals with Common Oxidants, Environ. Sci. Technol. 38 (2004) 3705–3712.
[18] G.P. Anipsitakis, D.D. Dionysiou, M.A. Gonzales, Cobalt mediated activation of peroxymonosulfate and sulfate radical attack on phenolic compounds. Implication of chloride ions, Environ. Sci. Technol. 40 (2006) 1000–1007.
[19] G.H. Rossetti, E.D. Albizzati, O.M. Alfano, Decomposition of formic acid in a water solution employing the photo-Fenton reaction, Ind. Eng. Chem. Res. 41 (2002) 1436–1444.
[20] N.A. Aristova, N. Karpel Vel Leitner, I.M. Piskarev, Degradation of formic acid in different oxidative processes, High Energy Chem. 36 (2002) 197–202.
[21] P.R. Gogate, S. Mujumdar, A.B. Pandit, Sonochemical reactors for waste water treatment: comparison using formic acid degradation as a model reaction, Adv. Environ. Res. 7 (2003) 283–299.
[22] N. Kang, D.S. Lee, J. Yoon, Kinetic modeling of Fenton oxidation of phenol and monochlorophenols, Chemosphere 47 (2002) 915–924.
[23] H. Gallard, J. De Laat, Kinetic modelling of Fe(III)/H_2 O_2 oxidation reactions in dilute aqueous solution using atrazine as a model organic compound, Water Res. 34 (12) (2000) 3107–3116.
[24] R. Andreozzi, A. D'Apuzzo, R. Marotta, A kinetic model for the degradation of benzothiazole by Fe^{3+}-photo-assisted Fenton process in a completely mixed batch reactor, J. Hazard. Mater. B80 (2000) 241–257.
[25] G.J. Price, A.A. Clifton, Sonochemical acceleration of persulfate decomposition, Polymer 37 (1996) 3971–3973.
[26] K. Okitsu, K. Iwasaki, Y. Yobiko, H. Bandow, R. Nishimura, Y. Maeda, Sonochemical degradation of azo dyes in aqueous solution: a new heterogeneous kinetics model taking into account the local concentration of OH radicals and azo dyes, Ultrason. Sonochem. 12 (2005) 255–262.
[27] G.V. Buxton, R.M. Sellers, Acid dissociation-constant of carboxyl radical-pulse-radiolysis studies of aqueous-solutions of formic-acid and sodium formate, J. Chem. Soc. Faraday Trans. 1 (69) (1973) 555–559.
[28] M. Lin, Y. Katsumura, Y. Muroya, H. He, T. Miyazaki, D. Hiroishi, Pulse radiolysis of sodium formate aqueous solution up to 400 °C: Absorption spectra, kinetics and yield of carboxyl radical $CO_2^{\bullet -}$, Radiat. Phys. Chem. 77 (2008) 1208–1212.
[29] I. Grčić, N. Koprivanac, D. Vujević, S. Papić, Removal of atrazine from simulated groundwater by AOTs, J. Adv. Oxid. Technol. 11 (1) (2008) 91–96.
[30] E. Neyens, J. Baeyens, A review of classic Fenton's peroxidation as an advanced oxidation technique, J. Hazard. Mater. 98 (2003) 33–50.
[31] S. Koda, T. Kimura, T. Kondo, H. Mitome, A standard method to calibrate sonochemical efficiency of an individual reaction system, Ultrason. Sonochem. 10 (2003) 149–156.
[32] S. Merouani, O. Hamdaoui, F. Saoudi, M. Chiha, Influence of experimental parameters on sonochemistry dosimetries: KI oxidation, Fricke reaction and H_2O_2 production, J. Hazard. Mater. 178 (2010) 1007–1014.
[33] K.R. Morison, C.A. Hutchinson, Limitations of the Weissler reaction as a model reaction for measuring the efficiency of hydrodynamic cavitation, Ultrason. Sonochem. 16 (2009) 176–183.
[34] R.F.P. Nogueira, M.C. Oliveira, W.C. Paterlini, Simple and fast spectrophotometric determination of H_2O_2 in photo-Fenton reactions using metavanadate, Talanta 66 (2005) 86–91.
[35] K.-C. Huang, R.A. Couttenye, G.E. Hoag, Kinetics of heat-assisted persulfate oxidation of methyl *tert*-butyl ether (MTBE), Chemosphere 49 (2002) 413–420.
[36] APHA, Standard Methods for the Examination of Water and Wastewater treatment, 20th ed., American Public Health Association, Washington, DC, USA, 1998.
[37] S. Ray, RSM: a statistical tool for process optimization, Ind. Tex. J. 117 (2006) 24–30.
[38] S. Bae, M. Shoda, Statistical optimization of culture conditions for bacterial cellulose production using Box–Behnken design, Biotechnol. Bioeng. 90 (2005) 20–28.
[39] T. Zhou, X. Lu, T.-T. Lim, Y. Li, F.-S. Wong, Degradation of chlorophenols (CPs) in an ultrasound-irradiated Fenton-like system at ambient circumstance: the QSPR (quantitative structure-property relationship) study, Chem. Eng. J. 156 (2010) 347–352.
[40] F. Chen, Y. Li, W. Cai, J. Zhang, Preparation and sono-Fenton performance of 4A-zeolite supported α-Fe_2O_3, J. Hazard. Mater. 177 (2010) 743–749.
[41] M. Ying-Shih, S. Chi-Fanga, L. Jih-Gaw, Degradation of carbofuran in aqueous solution by ultrasound and Fenton processes: Effect of system parameters and kinetic study, J. Hazard. Mater. 178 (2010) 320–325.
[42] K.P. Gopinath, K. Muthukumar, M. Velan, Sonochemical degradation of Congo red: Optimization through response surface methodology, Chem. Eng. J. 157 (2010) 427–433.
[43] K.S. Suslick, The chemical effect of ultrasound, Sci. Am. 260 (1989) 80–86.
[44] M.I. Pariente, F.A. Martinez, J.A. Melero, J. Ábotas, T. Velegraki, N.P. Xekoukoulotakis, D. Mantzavinos, Heterogeneous photo-Fenton oxidation of benzoic acid in water: effect of operating conditions, reaction by-products and coupling with biological treatment, Appl. Catal. B: Environ. 85 (2008) 24–32.
[45] K. Selvam, M. Muruganandham, M. Swaminathan, Enhanced heterogeneous ferrioxalate photo-fenton degradation of reactive orange 4 by solar light, Sol. Energy Mater. Sol. Cells 89 (2005) 61–74.
[46] B. Muthukumari, K. Selvam, I. Muthuvel, M. Swaminathan, Photoassisted hetero-Fenton mineralisation of azo dyes by Fe(II)-Al_2O_3 catalyst, Chem. Eng. J. 153 (2009) 9–15.
[47] O. Rozas, D. Contreras, M.A. Mondaca, M. Pérez-Moya, H.D. Mansilla, Experimental design of Fenton and photo-Fenton reactions for the treatment of ampicillin solutions, J. Hazard. Mater. 177 (2010) 1025–1030.
[48] I. Grčić, M. Mužic, D. Vujević, N. Koprivanac, Evaluation of atrazine degradation in UV/FeZSM-5/H_2O_2 system using factorial experimental design, Chem. Eng. J. 150 (2009) 476–484.
[49] T. Liu, H. You, Q. Chen, Heterogeneous photo-Fenton degradation of polyacrylamide in aqueous solution over Fe(III)–SiO_2 catalyst, J. Hazard. Mater. 162 (2009) 860–865.
[50] R.F.F. Pontes, J.E.F. Moraes, A. Machulek Jr., J.M. Pinto, A mechanistic kinetic model for phenol degradation by the Fenton process, J. Hazard. Mater. 176 (2010) 402–413.
[51] A.G. Chakinala, P.R. Gogate, A.E. Burgess, D.H. Bremmer, Industrial wastewater treatment using hydrodynamic cavitation and heterogeneous advanced Fenton processing, Chem. Eng. J. 152 (2009) 498–502.
[52] I. Grčić, D. Vujević, N. Koprivanac, The use of D-optimal design to model the effects of process parameters on mineralization and discoloration kinetics of Fenton-type oxidation, Chem. Eng. J. 157 (2010) 408–419.
[53] T.J. Mason, J.P. Lorimer, Applied Sonochemistry, Wiley-VCH Verlag GmbH, Weinheim, Germany, 2002.
[54] J. Farias, E.D. Albizzati, O.M. Alfano, Kinetic study of the photo-Fenton degradation of formic acid: combined effects of temperature and iron concentration, Catal. Today 144 (2009) 117–123.
[55] J. Lee, C. Lee, J. Yoon, High temperature dependence of 2, 4-dichlorophenoxyacetic acid degradation by Fe^{3+}/H_2O_2 system, Chemosphere 51 (2003) 963–971.
[56] N. Karpel Vel Leitner, M. Dore, Hydroxyl radical induced decomposition of aliphatic acids in oxygenated and deoxygenated aqueous solutions, J. Photochem. Photobiol. A 99 (1996) 137–143.
[57] M.R. Hoffmann, I. Hua, R. Höchemer, Application of ultrasonic irradiation for the degradation of chemical contaminants in water, Ultrason. Sonochem. 3 (1996) S163–S172.
[58] E.A. Coutsias, C. Seok, K.A. Dill, Using quaternions to calculate RMSD, J. Comput. Chem. 25 (2004) 1849–1857.